

NeRF-DetS: Enhancing Multi-View 3D Object Detection with Sampling-adaptive Network of Continuous NeRF-based Representation

Chi Huang¹, Xinyang Li¹, Shengchuan Zhang¹ *, Liujuan Cao¹, and Rongrong Ji¹

Key Laboratory of Multimedia Trusted Perception and Efficient Computing, Ministry of Education of China, Xiamen University, 361005, P.R. China.

Abstract. As a preliminary work, NeRF-Det unifies the tasks of novel view synthesis and 3D perception, demonstrating that perceptual tasks can benefit from novel view synthesis methods like NeRF, significantly improving the performance of indoor multi-view 3D object detection. Using the geometry MLP of NeRF to direct the attention of detection head to crucial parts and incorporating self-supervised loss from novel view rendering contribute to the achieved improvement. To better leverage the notable advantages of the continuous representation through neural rendering in space, we introduce a novel 3D perception network structure, NeRF-DetS. The key component of NeRF-DetS is the Multi-level Sampling-Adaptive Network, making the sampling process adaptively from coarse to fine. Also, we propose a superior multi-view information fusion method, known as Multi-head Weighted Fusion. This fusion approach efficiently addresses the challenge of losing multi-view information when using arithmetic mean, while keeping low computational costs. NeRF-DetS outperforms competitive NeRF-Det on the ScanNetV2 dataset, by achieving +5.02% and +5.92% improvement in mAP@.25 and mAP@.50, respectively.

Keywords: 3D Object Detection · NeRF · Multi-View

1 Introduction

3D object detection is a fundamental task for acquiring semantic and geometric information in 3D space. It aims to recognize and locate specific objects of certain classes in a 3D scene, which is widely utilized in applications such as Augmented Reality (AR) and Virtual Reality (VR), as well as in popular autonomous driving tasks [13, 15, 18, 19, 24, 38]. With the continuous advancement of technology, research on 3D perception has made significant progress, especially in the field of object detection. Currently, various sensors are widely used to obtain all kinds of information in space. Classical 3D object detection method [5, 28, 43] often relies on pre-reconstructed 3D representations or information from 3D sensors,

* Corresponding author

such as point clouds. However, the deployment costs of these approaches are substantially high. In this case, the most cost-effective way to acquire information from space is still through traditional RGB images. Therefore, exploring the relationship between posed RGB images and various potential information in 3D space has become a meaningful task to explore. In this paper, we focus on sufficiently utilizing the features of posed images to implement object detection in indoor spaces.

As a novel 3D representation, Neural Radiance Field [25] (NeRF) or NeRF-based method like Plenoxels [6] and IBRNet [35] have been introduced in spatial perception works [10, 16, 40]. In particular, NeRF-Det [40] has proposed an excellent structure that uses NeRF as an intermediate representation, allowing to explicitly model scene geometry as an opacity field by using the geometry MLP of NeRF. The utilization of NeRF as an intermediate spatial representation also improves the consistency of information extraction from multi-view images at the same spatial position. This dual-branch approach fully utilizes information as much as possible in the space, and most importantly, allows self-supervision of feature extraction from different camera views, ensuring the correctness and consistency of information extraction. However, if only fixed sampling is adopted, it is difficult to sufficiently leverage the consistency of information in scene, which is the notable feature introduced by NeRF in perception pipeline.

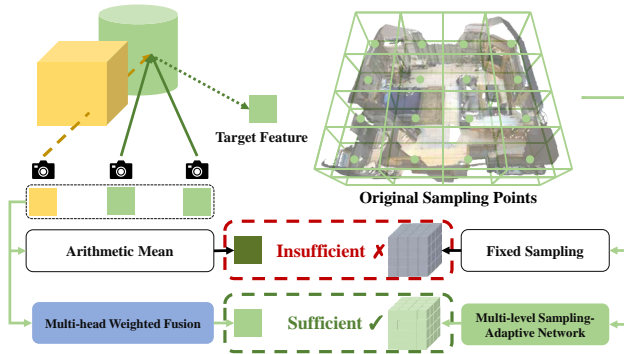


Fig. 1: Comparison between NeRF-Det [40] and NeRF-DetS.

Therefore, the multi-sampling strategy serves as a good solution for efficiently sampling extensive spatial information needed for the object detection task as much as possible. Currently, in the field of autonomous driving, the sparse and multi-level sampling strategy has become very popular and mature. In the scenarios of autonomous driving, object detection often relies on methods based on deformable DETR [44] like DETR3D [38], BEVformer [19] or similar approaches. In such scenarios, the general information density is relatively low. Scenes in au-

Autonomous driving are always at a large spatial scale, the size of most objects is large, and there is obvious distinction between objects. Also, most objects are distributed on the x-y plane, the accuracy requirement for the size of the z-axis space is not high. In these cases, many 3D detection methods can benefit from adopting a similar 2D structure. Therefore, the core problem of many 3D detection methods [12, 19, 21] in autonomous driving is to convert spatial information into information on the x-y plane like BEV or to supplement spatial information with weak 3D structures. However, there are notable differences between indoor and autonomous driving scenes. In indoor scenes, objects are often close to each other, exhibit significant size variations, have irregular spatial distributions, and involve multiple diverse object categories that need to be discerned. Directly utilizing a sparse sampling approach may result in the initial sampling points being incapable of precisely capturing key positional information and obtaining sufficient detailed data. Also, in autonomous driving tasks, the relative camera positions are fixed, and there are fewer overlapping viewpoints, limiting the availability of 3D information from multiple perspectives. Consequently, in indoor scenes with significant occlusions, it becomes crucial to fuse camera images with multiple overlapping viewpoints of the same sampling location in space. Using arithmetic mean would lead to confusion in sampled features due to occlusions among objects and other factors. Insufficient fusion limits the accurate acquisition of features in space. Hence, some current methods [35, 40] try to introduce non-parameterization of spatial feature variances during rendering process to guide the determination of occlusion relationships. However, such non-parameterization approaches have not yielded sufficient fusion results. If statistical results alone are considered as the final features, it would still dilute the information from those truly valuable viewpoints.

Therefore, we have considered the respective advantages and disadvantages of the scenarios and current methods. Instead of using the fixed-position sampling approach, we introduce the Multi-level Sampling-Adaptive Network. This network integrates the widely adopted adaptive sampling strategy into the dense sampling network structure. This modification enables us to sufficiently leverage the advantages of both the continuous feature in space and the consistency of information from multiple views at the same location when using the NeRF branch as supervision. In the prediction process of the preceding layer, predictions of the network not only include the classifications and bounding boxes in the spatial domain but also offsets. Subsequently, these offsets guide the sampling in the next layer. This enables the collection of information not captured by the fixed original sampling points and supplements the positional information of original sampling points. Consequently, this network effectively supplements information not covered by the original sampling points, enhancing the quality of detection boxes, particularly in terms of performance at high IoU threshold. Additionally, our approach incorporates an innovative multi-view fusion approach called Multi-Head Weighted Fusion. This approach predicts multi-head weights for a specific point from various spatial perspectives. We apply softmax processing on different perspectives, effectively fusing the information in space. This approach

efficiently integrates information throughout the entire space within reasonable computational complexity.

Based on our series of experiments, we find that by using our methods in NeRF-DetS, the results under the current dual-branch detection pipeline approach can be improved by +5.02% in mAP@.25 and +5.92% in mAP@.50. At the same time, we also compare the object detection accuracy under the IoU70 condition, and we achieve significant improvement compared to previous works.

2 Related Work

NeRF representation. 3D representation has gained significant attention since the original NeRF [25]. Early works, such as [1, 22, 31] used differentiable volumetric rendering to fit geometric and RGB information in 3D space with a network. NeuS [34] and VolSDF [41] improve the reconstruction quality by using SDF to replace density for better surface geometry reconstruction. Subsequent methods, especially Plenoxels [6] and 3DGS [17], have also demonstrated significant success in explicitly storing color and density features within the spatial domain. Instant-NGP [26] adopted a multi-resolution hash encoding as storage. These approaches have proven highly effective in leveraging multi-view posed images for robust 3D space reconstruction and generating high-quality novel view synthesis. Many works, including [3, 27, 35, 42] have also explored how to synthesize new views using a limited number of posed images. In particular, methods like IBRNet [35] and pixelNeRF [42] project 2D image features into 3D space, and decode the 3D feature into geometry and RGB information of positions in the 3D space. Inspired by this line of thought, NeRF-Det [40] projects ray samples onto the image plane, and demonstrated the effectiveness of such method.

3D object detection. With the advancement of autonomous driving technology and the increasing popularity of AR and VR devices, the development of 3D object detection [14, 20, 24] has been progressing rapidly. Many mature outdoor 3D detection methods focus on BEV (bird’s-eye view) perception such as BEVFormer [19], BEVDet [12], SparseBEV [21] and VCD [13]. After that, many occupancy reconstruction approaches like TPVFormer [15] and VoxFormer [18] have also been developed. DETR3D [38] and PETR [23] lift 2D features from multi-views into 3D to conduct 3D object detection based on DETR [2] and Deformable DETR [44]. Additionally, numerous methods have emerged for indoor detection, including RGB-D scan-based methods such as 3D-SIS [9], point cloud-based approaches like VoteNet [5] and FCAF3D [29]. ImVoxelNet [30] utilizes multi-view images to extract 2D features and project the feature from 2D to 3D, representing the 3D spatial as an voxel for perception.

Perception with NeRF. Numerous works [7, 10, 11, 16, 22, 40] have already incorporated NeRF into all kinds of perception tasks. In the context of 3D detection tasks, some earlier works [10, 16] first construct the scene into a NeRF representation and then perform perception on it. However, this approach requires reconstructing the entire scene in space before conducting perception, making it a non-end-to-end process that consumes significant time. Addition-

ally, some information may be lost during the reconstruction process. Recently, some works [11, 40] focus on improving perception performance with NeRF which have demonstrated its effectiveness. With the growing maturity of NeRF in 3D representation and a deeper exploration of its role in perception, NeRF-Det [40] first incorporates a NeRF branch into the pipeline of 3D object detection. The NeRF branch serves as an additional branch, using geometry MLP to predict the opacity of the sampling points. The opacity information helps the detection head to focus on areas with high opacity. Furthermore, NeRF branch fosters effective self-supervision among multi-view images. However, existing efforts have not sufficiently leveraged the advantages of introducing the NeRF branch, especially the continuity of features across the entire scene. Therefore, we propose NeRF-DetS to address this limitation.

3 Method

3.1 Overall detection process

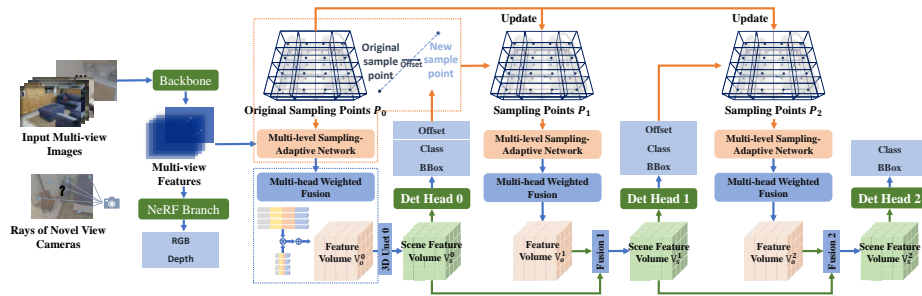


Fig. 2: Overview of NeRF-DetS. Our work mainly consists of two parts, namely Multi-level Sampling-Adaptive Network and Multi-Head Weighted Fusion. We will discuss the structure and implementation in this part with greater detail.

In this work, we present a novel method, NeRF-DetS, for 3D object detection that follows main pipeline of NeRF-Det. It takes only posed multi-view images as input and outputs a set of 3D bounding boxes that reveal the locations and classifications of objects in space. We randomly select N posed images for a given scene. These N multi-view images are fed into a 2D backbone to extract 2D features $F_i \in \mathbb{R}^{w \times h \times c}$, $i = 1, 2, 3, \dots, N$, w and h is the size of feature map, c is the feature dimension. Next, we uniformly sample spatial coordinates throughout the scene to obtain the original coordinate set as sample points $P_0 \in \mathbb{R}^{W \times L \times H \times 3}$. Here, W , L and H are the number of points sampled on xyz-axis. After sampling the feature in scene, we employ our proposed Multi-head Weighted Fusion to fuse the multi-view features volume from $V_m \in \mathbb{R}^{W \times L \times H \times c}$ into volume $V_s \in \mathbb{R}^{W \times L \times H \times c}$. After the feature volume passes the 3D U-Net,

we predict the bounding box, classification and offset by our proposed Adaptive Multi-layer Sampling Network. The offset is used for sampling supplement features effectively. The NeRF branch is used to generate the opacity of sampling points as NeRF-Det [40] do. Additionally, the NeRF branch ensures the continuity of features across the entire scene, which is sufficiently leveraged in our work.

3.2 Multi-level Sampling-Adaptive Network

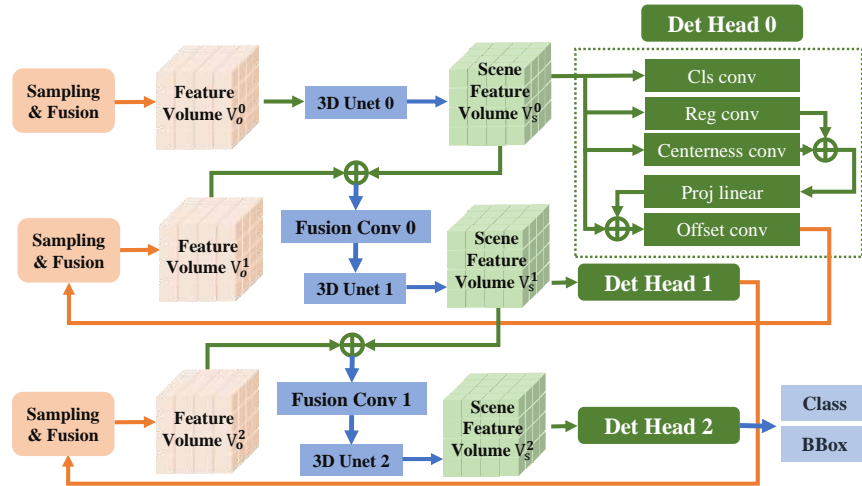


Fig. 3: Multi-level Sampling-Adaptive Network.

NeRF-Det [40] has demonstrated the effectiveness of the structure that combines perception with the NeRF branch. The perception branch ensures the feature extracted from images contains the semantic information. Due to the inherent nature of NeRF, the NeRF branch could enhance the consistency of information extraction from multi-view through self-supervision. Also, NeRF branch supervises the extraction of information in spatial terms for novel views, ensuring continuity of information in space. Additionally, the opacity generated from the NeRF branch helps the features focus on more important and relevant positions, thereby improving perception performance.

The continuity of the scene is the significant advantage of NeRF compared to other traditional reconstruction or NVS methods. This advantage allows NeRF to achieve high-quality novel view synthesis. Therefore, we propose the Multi-level Sampling-Adaptive Network, as illustrated in Fig. 3 to address how to

flexibly and efficiently utilize the continuous features in space to assist perception in dense sampling fashion.

First, we uniformly sample at voxel coordinate as the original sampling points P_0 . After sampling and fusion, we can obtain a feature volume V_o^0 . We pass it through a 3D U-Net to get V_s^0 , which represents the spatial scene. In our Multi-level Sampling-Adaptive Network, we not only use the detection head to predict the bounding box and class of objects in the space, like other FCOS3D [36]-like methods do, but also use the detection head to predict the offset of the next layer sampling points relative to the original sampling points. We concatenate the input scene features V_s^0 with the predicted results from the regression convolution layer and the centerness convolution layer after linear mapping. The concatenated features then undergo the offset convolution layer to predict offsets, as shown in the first row of the Fig. 3. To obtain the sample points P_1 of the first layer, we use the original sampling points P_0 and the predicted offsets. For each $\mathbf{p}' \in P_1$, $\mathbf{p}' = \mathbf{p} + \Delta\mathbf{p}$, where $\mathbf{p} \in P_0$.

Through the same sampling and fusion, we can obtain V_o^1 , representing the feature volume sampled on the first-level sampling points P_1 after the offset. After concatenating V_o^1 with the feature volume V_s^0 , we use a shallow fusion convolution layer and a 3D U-net with the same structure to get feature volume of first layer V_s^1 . After obtaining the new feature volume V_s^1 , we follow exactly the same process to obtain V_s^2 , by predicting the bounding boxes and classifications of objects in the scene, as well as the offsets of the next layer. This process continues iteratively. In our work, we use two levels. By employing two levels of iteration, we mitigate the potential uncertainty in offsets that may misguide the original features. This multi-layer approach ensures more accurate sampling and enables us to gather abundant information for improved results.

In our approach, the unfixed Multi-level Sampling-Adaptive Network structure is employed, we utilize previously sampled information to predict the positions of subsequent samples. This process aims to supplement the missing information in the original sample positions and enable the entire feature volume to efficiently capture spatially relevant information, even in scenarios with low sampling resolution. Our method incorporates an adaptive sampling process that adapts to the missing information in space. Through a two-level process, we obtain the final feature volume V_s^2 . This feature volume is then passed into our detection head, which generates the final predictions for classification, location, and centerness by classification, regression and centerness convolution layers respectively. To make sure that every layer learns the right semantic and contributes to predicting better sample offsets, we supervise the predicted results of each layer.

3.3 Multi-head Weighted Fusion

The sampling and fusion strategy of multiple perspectives is crucial for perception. For each sample point $\mathbf{p} \in P_0$, and each feature map F_i , we use bilinear interpolation $\text{Bilinear}((u_i, v_i), F_i)$ to sample the features in 2D space, where u_i , v_i is pixel coordinates projected from \mathbf{p} to F_i . For any invalid sample points

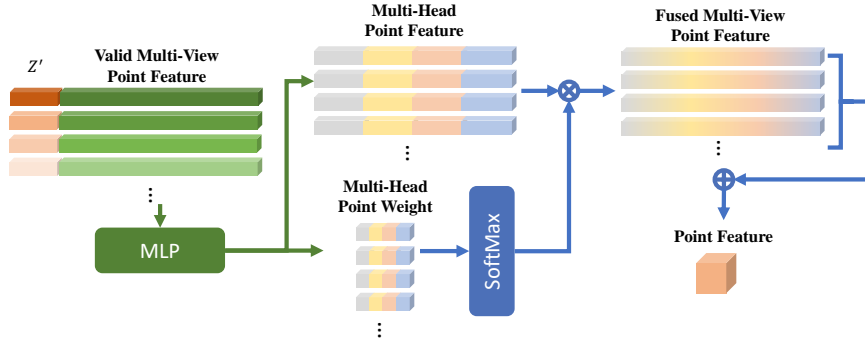


Fig. 4: Multi-head Weighted Fusion Process.

located outside or behind the feature plane F_i are set them to $\mathbf{0}$. After obtaining the preliminary multi-view feature volume $V_m \in \mathbb{R}^{N \times W \times H \times L \times c}$ in space, we need to convert them into a scene feature volume $V_o \in \mathbb{R}^{W \times H \times L \times c}$ to fuse valid information from different views for subsequent processing.

In the current mainstream sparse 3D detection methods, attention mechanisms [32] with $\text{Attention}(Q, K, V) = \text{softmax}\left(\frac{QK^T}{\sqrt{d_k}}\right)V$, are widely used to handle fusion features of different views or interact features from different sampling points. This global approach allows for comprehensive fusion of information from different views and different position. This approach has widely used. Nonetheless, its extensive computational resource requirements, making it unsuitable for scenarios involving multiple perspectives and dense sampling.

In this case, in NeRF-Det, the valid features from multi-views are directly fused using an arithmetic mean. Simply let $V_o = \frac{1}{N} \times \sum_{i=1}^N V_{m_i}$. The advantage of this approach is that it can quickly and directly fuse information from multi-views without occupying additional computational resource. However, this approach lacks effective interaction between features of the same sampling point across different views. When the weights are equivalent across all views, minority salient information may not be fully reflected in the final spatial features. Therefore, we propose a multi-head parameterized fusion strategy, called Multi-head Weighted Fusion. It simplifies the weight calculation process and enables better fusion of information from different perspectives by using weights.

In NeRF-DetS, we not only obtain the multi-view feature volume V_m of the sampling points in the scene space, but also the distance from each sampling point to the camera position, denoted as $Z \in \mathbb{R}^{N \times W \times H \times L \times 1}$. The distance Z is encoded into $Z' \in \mathbb{R}^{N \times W \times H \times L \times c'}$ through an encoder function, denoted as $\text{Encoder}(z) = \sin(A \times \text{Linear}(z))$, where A represents a constant. This allows the sampled features to incorporate the distance information from the sampling points to the 2D feature plane, leading to improved fusion.

By concatenating the features of the sampling points and Z' , we pass them into a linear layer to obtain the output feature volume $V'_m \in \mathbb{R}^{N \times W \times H \times L \times n \times c/n}$ and the multi-head weight $W \in \mathbb{R}^{N \times W \times H \times L \times n}$. In our work, the number of multi-head weights is set to $n = 8$. The softmax function is then applied to the multi-head weight tensor along the dimension of multi-views to obtain the multi-head weights across different views in the entire space. The V'_m in the space is then multiplied by the multi-head weights to obtain the final V_o .

$$W' = \text{SoftMax}(W), V_o = \sum_{i=1}^N W'_i \times V'_{m_i} \quad (1)$$

Through the process of multi-head weight sampling, we can ensure that a small number of truly useful perspective information obtains higher weights while reasonably utilizing the GPU memory. In this way, the feature fusion process will be more focused on extracting truly effective information from the space.

3.4 Training Objective

Throughout our entire training process, we adopt the identical loss structure as NeRF-Det [40]. In the detection branch, we supervise classification, location, and centerness like the ImVoxelNet [30] using FCOS3D [36]-structured head. As we use Multi-level Sampling-Adaptive Network, we supervise the output of every level. This ensures that every layer comprehends spatial information while aiding in improving prediction of offsets for subsequent layers. In NeRF branch, we supervise depth and RGB to capture information in the space. Therefore, in our training process, we use a total of three levels of losses $L_{cls}, L_{cntr}, L_{loc}$ for classification loss, centerness loss, and localization loss, to supervise the detection process. In the NeRF branch, we use RGB and depth losses L_c and L_d , $L_c = \|\hat{C}(r) - \hat{C}_{gt}(r)\|_2$, $L_d = \|D(r) - D_{gt}(r)\|$. NeRF branch only needs to render RGB during training, and during inference, it only requires the geometry MLP to output the density of positions in space.

$$L = \sum_{i=1}^3 (L_{cls_i} + L_{cntr_i} + L_{loc_i}) + L_c + L_d \quad (2)$$

4 Experiment Result

In our experiment, we follow the entire structure of NeRF-Det [40], aiming to validate the effectiveness of our proposed methods in improving high-quality object detection within the framework of the NeRF branch while minimizing modifications to the original network architecture. We perform experiments in ScannetV2 [4]. Which is a widely used dataset in indoor object detection or other indoor perception tasks. It contains 1513 indoor scenes of various kinds of indoor

Methods	cab	bed	chair	sofa	table	door	wind	bkslf	pic	cntr	desk	curt	fridge	shwr	toil	sink	bath	ofurn	mAP@.25	mAP@.50
Seg-Cluster [37]	11.8	13.5	18.9	14.6	13.8	11.1	11.5	11.7	0.0	13.7	12.2	12.4	11.2	18.0	19.5	18.9	16.4	12.2	13.4	-
Mask R-CNN [8]	15.7	15.4	16.4	16.2	14.9	12.5	11.6	11.8	19.5	13.7	14.4	14.7	21.6	18.5	25.0	24.5	24.5	16.9	17.1	10.5
SGPN [37]	20.7	31.5	31.6	40.6	31.9	16.6	15.3	13.6	0.0	17.4	14.1	22.2	0.0	0.0	72.9	52.4	0.0	18.6	22.2	-
3D-SIS [9]	19.8	69.7	66.2	71.8	36.1	30.6	10.9	27.3	0.0	10.0	46.9	14.1	53.8	36.0	87.6	43.0	84.3	16.2	40.2	22.5
VoteNet [5]	36.3	87.9	88.7	89.6	58.8	47.3	38.1	44.6	7.8	56.1	71.7	47.2	45.4	57.1	94.9	54.7	92.1	37.2	58.7	33.5
FCAF3D [29]	57.2	87.0	95.0	92.3	70.3	61.1	60.2	64.5	29.9	64.3	71.5	60.1	52.4	83.9	99.9	84.7	86.6	65.4	71.5	57.3
CAGroup3D [33]	60.4	93.0	95.3	92.3	69.9	67.9	63.6	67.3	40.7	77.0	83.9	69.4	65.7	73.0	100	79.7	87.0	66.1	75.1	61.3
ImVoxelNet [30]	34.5	83.6	72.6	71.6	54.2	30.3	14.8	42.6	0.8	40.8	65.3	18.3	52.2	40.9	90.4	53.3	74.9	33.1	48.4	23.7
NeRF-Det* [40]	37.7	84.1	74.5	71.8	54.2	34.2	17.4	51.6	0.1	54.2	71.3	16.7	54.5	55.0	92.1	50.7	73.8	34.1	51.8	27.4
NeRF-Det+* [11]	38.9	83.9	73.9	77.6	57.2	33.3	23.5	47.9	1.5	56.9	77.7	21.1	61.5	46.8	92.8	49.2	80.2	34.5	53.2	29.6
NeRF-DetS*(Ours)	43.7	83.8	78.3	83.0	56.8	43.2	28.8	52.0	3.8	70.5	69.8	28.5	59.4	61.6	93.1	52.4	83.3	44.5	57.6	35.6

Table 1: Quantitative comparison on ScanNetV2. The above block shows the methods that base on the point cloud or RGBD input. The block below shows methods base on the multi-view RGB images input. * indicates the method with depth supervision. For the methods base on the multi-view RGB images, we all evaluate on the result of ResNet50. We assess performance of each category using mAP@0.25 as the evaluation metric. We use bold to highlight the method in best performance of each category.

rooms. Following the official separation, we use 1201 scenes for training and 312 scenes for validation and testing. We use official tools provided by MMDetection3D, randomly choose 300 RGB images and their corresponding depth images in resolution 320×240 for each scene. Note that the depth is only used in the training process to supervise the output of the NeRF branch. For each scene, we separately use 50 and 101 images randomly chosen from the processed 300 images for training and testing. Due to the simplicity of the original network architecture, the training process converges rapidly. In our experiment, we increase the number of epochs by an additional 50% to ensure that the performance of the methods we compared on NeRF-Det [40] does not suffer from overfitting while allowing our proposed methods to converge effectively. This training strategy allows for a more accurate evaluation of network performance and provides more reliable results for our research. We evaluate the performance of methods by mean Average Precision (mAP) and mean Average Recall (mAR) at 0.25 IoU, 0.5 IoU and 0.7 IoU threshold, denoted by mAP@.25 / mAP@.50 / mAP@.70, mAR@.25 / mAR@.50 / mAR@.70.

We use ResNet50 as the backbone for our experiment. We use NeRF-Det [40] with ResNet50 and depth-supervision as our baselines for comparison in Table 2. Under our training strategy, after applying our full method, compared to our baseline, we have made significant improvements, with AP under IOU25 by +5.02% and AP under IOU50 by +5.92%. This indicates that our method can effectively enhance object detection performance. The improvement, especially in the IoU50 metric, demonstrates that our method is capable of better integrating spatial information from multi-view and adaptively sample to supplement the original sample points. By employing an adaptive sampling approach, we have greatly enhanced the effectiveness of the sampling process. In addition to these two metrics, we also evaluate the detection performance at a high threshold, IOU70, which is used as metric in PARQ [39]. Our method completely outperformed the results obtained from the previous fixed sampling approaches or works, demonstrating its ability to effectively supplement missing information in the original pipeline and improve the quality of our predicted bounding boxes.

metrics	mAP@.25		mAR@.25		mAP@.50		mAR@.50		mAP@.70		mAR@.70	
	NeRF-Det	Ours	NeRF-Det	Ours	NeRF-Det	Ours	NeRF-Det	Ours	NeRF-Det	Ours	NeRF-Det	Ours
toilet	92.59	93.10	93.10	93.10	77.60	83.60	79.31	84.48	27.60	45.26	36.21	50.00
bed	81.53	83.84	83.95	86.42	70.52	72.57	74.07	76.54	38.91	43.76	44.44	50.62
bathhtub	80.22	83.34	83.87	87.10	71.76	76.18	74.19	80.65	34.45	30.47	41.94	45.16
sofa	78.56	83.07	86.60	90.72	50.77	63.13	59.79	71.13	15.82	29.85	25.77	41.24
chair	73.98	78.31	80.70	83.19	43.33	53.52	53.00	61.18	10.01	16.39	21.05	29.17
desk	66.84	69.65	88.98	88.98	42.32	45.61	66.93	68.50	14.11	22.60	33.07	43.31
table	54.61	56.84	73.14	75.43	40.03	43.36	55.71	60.00	11.32	15.32	23.14	31.71
refrigerator	60.29	59.39	68.42	73.68	24.67	40.81	42.11	50.88	04.00	03.23	10.53	10.53
sink	54.70	52.39	63.27	63.27	27.06	33.74	32.65	42.86	08.48	17.42	14.29	21.43
bookshelf	46.65	51.95	70.13	79.22	19.75	28.58	32.47	51.95	05.63	05.04	09.09	18.18
showercurtrain	52.32	61.64	71.43	82.14	03.35	10.84	21.43	28.57	00.13	00.00	03.57	00.00
counter	45.20	70.50	67.31	86.54	15.91	22.67	28.85	38.46	00.31	00.58	03.85	07.69
cabinet	39.49	43.71	63.44	65.32	16.03	18.61	33.33	36.29	02.68	04.85	08.87	11.02
door	35.78	43.15	55.67	61.24	09.19	15.76	23.77	29.76	00.55	02.05	03.43	07.71
garbagebin	36.99	44.51	54.15	58.68	15.75	21.74	29.62	33.77	01.99	03.83	06.42	11.51
curtain	21.19	28.47	53.73	44.78	02.80	03.57	10.45	08.96	00.12	00.50	01.49	01.49
window	23.62	28.77	42.91	48.94	03.03	05.71	12.06	16.67	00.24	01.26	01.42	03.55
picture	01.46	03.79	09.91	16.22	00.56	00.97	04.05	05.41	00.00	00.02	00.45	00.45
Overall	52.56	57.58	67.26	71.39	29.69	35.61	40.77	47.00	09.80	13.47	16.06	21.38

Table 2: Compared with NeRF-Det [40]

4.1 Resolution study

Table 3 presents the performance evaluation of our method at various resolutions, aiming to assess its robustness and efficiency under different spatial sampling configurations. The first row is our method, which involves two additional levels of spatial sampling, resulting in a higher resolution of $40 \times 40 \times 16$. In this configuration, the total number of sampling points is tripled compared to the original NeRF-Det [40] method. Here, 16 represents the vertical resolution in space. The subsequent rows illustrate the impact of altering the resolution in specific dimensions. The "3/2" column reflects a change in the vertical resolution to 8, while the "3/4" column indicates a decrease in the horizontal resolution to 20. Similarly, the "3/8" column represents a halving of the both horizontal and vertical resolution in space. These variations allow us to analyze how changes in resolution influence the performance of our method. For reference, the "Org 1/2", "Org 1/4" and "Org 1/8" columns depict the performance of the original NeRF-Det [40] method when adapting to reduced resolutions.

	AP25	AR25	AP50	AR50	AP70	AR70
Ours	57.58	71.39	35.61	47.00	13.47	21.38
NeRF-Det	52.56	67.26	29.69	40.77	09.80	16.06
Ours 3/2	54.31	68.44	28.86	41.40	10.60	18.00
NeRF-Det 1/2	49.74	65.93	26.06	38.28	07.77	14.05
Ours 3/4	51.60	66.19	29.60	40.54	09.95	16.57
NeRF-Det 1/4	46.75	61.61	25.15	34.15	07.85	13.81
Ours 3/8	50.86	63.36	29.09	38.97	10.77	17.18
NeRF-Det 1/8	44.65	58.33	23.91	32.81	07.80	12.97

Table 3: Performance compare with NeRF-Det in different resolution.

In our experiment, we utilize multiple levels of adaptive sampling to sample features in the spatial domain. Compared with NeRF-Det, we find that our method excels in enhancing the sampling of effective positional information in low-resolution cases, which supplements for the information missed by the original sampling points. Simultaneously, we observe a positive correlation between the AR and the number of sampling points, indicating that AR tends to increase with higher sampling density. Notably, when comparing the improvement in mAR@.25 with mAR@.50, we find that the enhancement at threshold IoU 50 surpassed that at threshold IoU 25. This observation underscores the efficacy of our method in facilitating a more substantial improvement in high-quality detection results. By exclusively employing 3/8 or 3/4 sampling points of the original NeRF-Det [40], we achieve performance that are comparable to or even surpass those obtained with NeRF-Det [40] in terms of threshold 50. This not only reduces the computational cost associated with spatial sampling but also underscores the robustness of our adaptive sampling strategy in maintaining high-quality detection. Furthermore, threshold at IoU 70, even with our lowest resolution sampling points, our method outperforms the NeRF-Det [40]. This capability enables our model to effectively distinguish objects in challenging scenarios, such as overlapping or partially occluded targets, through adaptive sampling. Consequently, our approach maintains outstanding detection accuracy in complex spatial environments.

4.2 Ablation study

We test the influence of Multi-head Weighted Fusion on the entire detection process. Compared to directly averaging the features at a position, a more reasonable fusion approach greatly enhanced the detection process.

	mAP@.25	mAR@.25	mAP@.50	mAR@.50	mAP@.70	mAR@.70
NeRF-Det	52.56	67.26	29.69	40.77	09.80	16.06
+MWF	55.69	70.80	32.07	43.79	10.20	16.73
+Flip	56.73	73.08	34.49	46.16	12.35	19.22
+1 Level	57.39	70.89	34.71	45.92	12.62	21.01
+2 Level	57.58	71.39	35.61	47.00	13.47	21.38

Table 4: Ablation

In Table 4, we present the performance metrics for different configurations in NeRF-DetS. We incrementally introduce various improvements, including NeRF-Det, +MWF (Multi-head Weighted Fusion), +Flip, +1 Level, and +2 Level. Each configuration is evaluated for detection performance at three IoU thresholds (0.25, 0.50, and 0.70). From the table, it is evident that with the gradual introduction of improvements, there is a significant enhancement in detection performance. NeRF-Det, as our baseline, achieves commendable performance across all IoU thresholds. The introduction of +MWF further improves

both mAP and mAR. +Flip and +1 Level configurations also show further enhancements, although +1 Level exhibits a slight decrease in mAP@0.50 and mAR@0.50 compared to +Flip. For the +2 Level configuration, we observe the best performance across all IoU thresholds. This indicates that introducing two additional levels of adaptive sampling contributes to improving the robustness and accuracy of the detection model in NeRF-DetS. Specifically, the adoption of a 2-level adaptive offset sampling approach helps address the significant uncertainty that may arise from a 1-level adaptive offset. This uncertainty could result in ineffective or incorrect features, impacting the final detection performance by sampling positions irrelevant to the object itself.

In our experiments, we introduce flip augmentation by horizontally flipping the posed images and their corresponding depths. Additionally, we mirror-reflect the camera extrinsics along the x-y plane. This simple approach not only allows us to mirror-flip the 2D images but also mirror-transforms the sampled 3D voxels. In the entire pipeline, whether it is a 2D or 3D network, this method facilitates the convenient augmentation for the diversity of input to the network, enhancing the robustness of the network, aiding better object detection by the model.

	mAP@.25	mAR@.25	mAP@.50	mAR@.50	mAP@.70	mAR@.70
With offset	57.58	71.39	35.61	47.00	13.47	21.38
Without offset	51.57	66.47	28.37	39.92	11.01	17.85

Table 5: Offset Ablation

We attempt to retain all network components but abandon the spatial sampling process using offsets, shown in Tabel 5. Which means we sample points for three times at the same positions. We find that despite the increased number of parameters, there is no improvement in performance, and it even lead to a decline in performance. This confirms that the offsets indeed capture useful information from other positions in space to supplement the features of the original sampling positions, thereby improving the final performance.

4.3 Qualitative results

We present our visualized results in fig. 5. As shown in the figure, our method is capable of achieving more accurate and higher-quality object detection in various spatial environments. In scenes with densely packed objects, some detection results of NeRF-Det are not even accurate enough to locate the objects, with significant bounding box offsets for many objects, particularly in locations with fewer perspectives where accurate bounding box positions cannot be predicted. Also, we can observe that for larger-scale objects, such as large sofas and tables, NeRF-Det [40] often fails to provide accurate bounding boxes to encompass the entire object due to insufficient interaction of information between different positions.

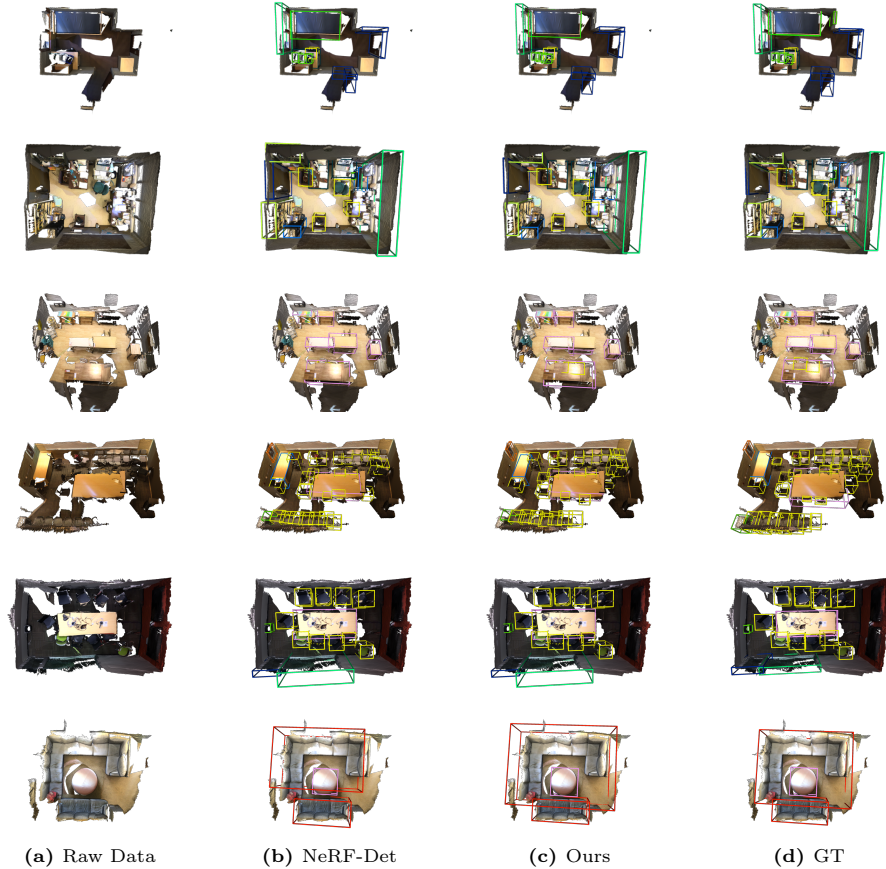


Fig. 5: Visual comparison between NeRF-Det and NeRF-DetS. The input we use is only multi-view posed RGB images, the mesh is only for visualization.

5 Conclusion

This paper introduces the NeRF-DetS to enhance the performance of object detection for multi-view images in the continuous NeRF-based representation. To sufficiently leverage the advantages brought by the NeRF branch to the perceptual process, we employ the Multi-level Sampling-Adaptive Network, which fully use the notable characteristic of the continuity in NeRF-based representation. Additionally, recognizing shortcomings in the fusion of multi-view information in space, we propose the Multi-head Weighted Fusion. This approach utilizes weights to address situations where a particular viewpoint in space may be occluded in the presence of multiple perspectives. Extensive experiments on the ScanNetV2 dataset validate the effectiveness of our method in improving the performance of detection tasks.

References

1. Barron, J.T., Mildenhall, B., Tancik, M., Hedman, P., Martin-Brualla, R., Srinivasan, P.P.: Mip-nerf: A multiscale representation for anti-aliasing neural radiance fields. In: Proceedings of the IEEE/CVF International Conference on Computer Vision. pp. 5855–5864 (2021) [4](#)
2. Carion, N., Massa, F., Synnaeve, G., Usunier, N., Kirillov, A., Zagoruyko, S.: End-to-end object detection with transformers. In: European conference on computer vision. pp. 213–229. Springer (2020) [4](#)
3. Chen, A., Xu, Z., Zhao, F., Zhang, X., Xiang, F., Yu, J., Su, H.: Mvsnerf: Fast generalizable radiance field reconstruction from multi-view stereo. In: Proceedings of the IEEE/CVF International Conference on Computer Vision. pp. 14124–14133 (2021) [4](#)
4. Dai, A., Chang, A.X., Savva, M., Halber, M., Funkhouser, T., Nießner, M.: Scannet: Richly-annotated 3d reconstructions of indoor scenes. In: Proceedings of the IEEE conference on computer vision and pattern recognition. pp. 5828–5839 (2017) [9](#)
5. Ding, Z., Han, X., Niethammer, M.: Votenet: A deep learning label fusion method for multi-atlas segmentation. In: Medical Image Computing and Computer Assisted Intervention–MICCAI 2019: 22nd International Conference, Shenzhen, China, October 13–17, 2019, Proceedings, Part III 22. pp. 202–210. Springer (2019) [1](#), [4](#), [10](#)
6. Fridovich-Keil, S., Yu, A., Tancik, M., Chen, Q., Recht, B., Kanazawa, A.: Plenoxels: Radiance fields without neural networks. In: Proceedings of the IEEE/CVF Conference on Computer Vision and Pattern Recognition. pp. 5501–5510 (2022) [2](#), [4](#)
7. Fu, X., Zhang, S., Chen, T., Lu, Y., Zhu, L., Zhou, X., Geiger, A., Liao, Y.: Panoptic nerf: 3d-to-2d label transfer for panoptic urban scene segmentation. In: 2022 International Conference on 3D Vision (3DV). pp. 1–11. IEEE (2022) [4](#)
8. He, K., Gkioxari, G., Dollár, P., Girshick, R.: Mask r-cnn. In: Proceedings of the IEEE international conference on computer vision. pp. 2961–2969 (2017) [10](#)
9. Hou, J., Dai, A., Nießner, M.: 3d-sis: 3d semantic instance segmentation of rgb-d scans. In: Proceedings of the IEEE/CVF conference on computer vision and pattern recognition. pp. 4421–4430 (2019) [4](#), [10](#)
10. Hu, B., Huang, J., Liu, Y., Tai, Y.W., Tang, C.K.: Nerf-rpn: A general framework for object detection in nerfs. In: Proceedings of the IEEE/CVF Conference on Computer Vision and Pattern Recognition. pp. 23528–23538 (2023) [2](#), [4](#)
11. Huang, C., Hou, Y., Ye, W., Huang, D., Huang, X., Lin, B., Cai, D., Ouyang, W.: Nerf-det++: Incorporating semantic cues and perspective-aware depth supervision for indoor multi-view 3d detection. arXiv preprint arXiv:2402.14464 (2024) [5](#), [10](#)
12. Huang, J., Huang, G., Zhu, Z., Ye, Y., Du, D.: Bevdet: High-performance multi-camera 3d object detection in bird-eye-view. arXiv preprint arXiv:2112.11790 (2021) [3](#), [4](#)
13. Huang, L., Li, Z., Sima, C., Wang, W., Wang, J., Qiao, Y., Li, H.: Leveraging vision-centric multi-modal expertise for 3d object detection. Advances in Neural Information Processing Systems **36** (2024) [1](#), [4](#)
14. Huang, L., Wang, H., Zeng, J., Zhang, S., Cao, L., Ji, R., Yan, J., Li, H.: Geometric-aware pretraining for vision-centric 3d object detection. arXiv preprint arXiv:2304.03105 (2023) [4](#)
15. Huang, Y., Zheng, W., Zhang, Y., Zhou, J., Lu, J.: Tri-perspective view for vision-based 3d semantic occupancy prediction. In: Proceedings of the IEEE/CVF Con-

- ference on Computer Vision and Pattern Recognition. pp. 9223–9232 (2023) [1](#), [4](#)
16. Jeong, Y., Shin, S., Lee, J., Choy, C., Anandkumar, A., Cho, M., Park, J.: Perception: Perception using radiance fields. *Advances in Neural Information Processing Systems* **35**, 26105–26121 (2022) [2](#), [4](#)
 17. Kerbl, B., Kopanas, G., Leimkühler, T., Drettakis, G.: 3d gaussian splatting for real-time radiance field rendering. *ACM Transactions on Graphics* **42**(4) (2023) [4](#)
 18. Li, Y., Yu, Z., Choy, C., Xiao, C., Alvarez, J.M., Fidler, S., Feng, C., Anandkumar, A.: Voxformer: Sparse voxel transformer for camera-based 3d semantic scene completion. In: *Proceedings of the IEEE/CVF Conference on Computer Vision and Pattern Recognition*. pp. 9087–9098 (2023) [1](#), [4](#)
 19. Li, Z., Wang, W., Li, H., Xie, E., Sima, C., Lu, T., Qiao, Y., Dai, J.: Bevformer: Learning bird’s-eye-view representation from multi-camera images via spatiotemporal transformers. In: *European conference on computer vision*. pp. 1–18. Springer (2022) [1](#), [2](#), [3](#), [4](#)
 20. Liu, H., Lu, T., Xu, Y., Liu, J., Li, W., Chen, L.: Camliflow: Bidirectional camera-lidar fusion for joint optical flow and scene flow estimation. In: *Proceedings of the IEEE/CVF Conference on Computer Vision and Pattern Recognition*. pp. 5791–5801 (2022) [4](#)
 21. Liu, H., Teng, Y., Lu, T., Wang, H., Wang, L.: Sparsebev: High-performance sparse 3d object detection from multi-camera videos. In: *Proceedings of the IEEE/CVF International Conference on Computer Vision*. pp. 18580–18590 (2023) [3](#), [4](#)
 22. Liu, L., Gu, J., Zaw Lin, K., Chua, T.S., Theobalt, C.: Neural sparse voxel fields. *Advances in Neural Information Processing Systems* **33**, 15651–15663 (2020) [4](#)
 23. Liu, Y., Wang, T., Zhang, X., Sun, J.: Petr: Position embedding transformation for multi-view 3d object detection. In: *European Conference on Computer Vision*. pp. 531–548. Springer (2022) [4](#)
 24. Liu, Z., Tang, H., Amini, A., Yang, X., Mao, H., Rus, D.L., Han, S.: Bevfusion: Multi-task multi-sensor fusion with unified bird’s-eye view representation. In: *2023 IEEE international conference on robotics and automation (ICRA)*. pp. 2774–2781. IEEE (2023) [1](#), [4](#)
 25. Mildenhall, B., Srinivasan, P.P., Tancik, M., Barron, J.T., Ramamoorthi, R., Ng, R.: Nerf: Representing scenes as neural radiance fields for view synthesis. *Communications of the ACM* **65**(1), 99–106 (2021) [2](#), [4](#)
 26. Müller, T., Evans, A., Schied, C., Keller, A.: Instant neural graphics primitives with a multiresolution hash encoding. *ACM Transactions on Graphics (ToG)* **41**(4), 1–15 (2022) [4](#)
 27. Niemeyer, M., Barron, J.T., Mildenhall, B., Sajjadi, M.S., Geiger, A., Radwan, N.: Regnerf: Regularizing neural radiance fields for view synthesis from sparse inputs. In: *Proceedings of the IEEE/CVF Conference on Computer Vision and Pattern Recognition*. pp. 5480–5490 (2022) [4](#)
 28. Qi, C.R., Su, H., Mo, K., Guibas, L.J.: Pointnet: Deep learning on point sets for 3d classification and segmentation. In: *Proceedings of the IEEE conference on computer vision and pattern recognition*. pp. 652–660 (2017) [1](#)
 29. Rukhovich, D., Vorontsova, A., Konushin, A.: Fcaf3d: Fully convolutional anchor-free 3d object detection. In: *European Conference on Computer Vision*. pp. 477–493 (2022) [4](#), [10](#)
 30. Rukhovich, D., Vorontsova, A., Konushin, A.: Imvoxelnet: Image to voxels projection for monocular and multi-view general-purpose 3d object detection. In: *Proceedings of the IEEE/CVF Winter Conference on Applications of Computer Vision*. pp. 2397–2406 (2022) [4](#), [9](#), [10](#)

31. Sun, C., Sun, M., Chen, H.T.: Direct voxel grid optimization: Super-fast convergence for radiance fields reconstruction. In: Proceedings of the IEEE/CVF Conference on Computer Vision and Pattern Recognition. pp. 5459–5469 (2022) [4](#)
32. Vaswani, A., Shazeer, N., Parmar, N., Uszkoreit, J., Jones, L., Gomez, A.N., Kaiser, Ł., Polosukhin, I.: Attention is all you need. *Advances in neural information processing systems* **30** (2017) [8](#)
33. Wang, H., Dong, S., Shi, S., Li, A., Li, J., Li, Z., Wang, L., et al.: Cagroup3d: Class-aware grouping for 3d object detection on point clouds. *Advances in Neural Information Processing Systems* **35**, 29975–29988 (2022) [10](#)
34. Wang, P., Liu, L., Liu, Y., Theobalt, C., Komura, T., Wang, W.: Neus: Learning neural implicit surfaces by volume rendering for multi-view reconstruction. *arXiv preprint arXiv:2106.10689* (2021) [4](#)
35. Wang, Q., Wang, Z., Genova, K., Srinivasan, P.P., Zhou, H., Barron, J.T., Martin-Brualla, R., Snavely, N., Funkhouser, T.: Ibrnet: Learning multi-view image-based rendering. In: Proceedings of the IEEE/CVF Conference on Computer Vision and Pattern Recognition. pp. 4690–4699 (2021) [2](#), [3](#), [4](#)
36. Wang, T., Zhu, X., Pang, J., Lin, D.: Fcos3d: Fully convolutional one-stage monocular 3d object detection. In: Proceedings of the IEEE/CVF International Conference on Computer Vision. pp. 913–922 (2021) [7](#), [9](#)
37. Wang, W., Yu, R., Huang, Q., Neumann, U.: Sgpn: Similarity group proposal network for 3d point cloud instance segmentation. In: Proceedings of the IEEE conference on computer vision and pattern recognition. pp. 2569–2578 (2018) [10](#)
38. Wang, Y., Guizilini, V.C., Zhang, T., Wang, Y., Zhao, H., Solomon, J.: Detr3d: 3d object detection from multi-view images via 3d-to-2d queries. In: Conference on Robot Learning. pp. 180–191. PMLR (2022) [1](#), [2](#), [4](#)
39. Xie, Y., Jiang, H., Gkioxari, G., Straub, J.: Pixel-aligned recurrent queries for multi-view 3d object detection. In: Proceedings of the IEEE/CVF International Conference on Computer Vision. pp. 18370–18380 (2023) [10](#)
40. Xu, C., Wu, B., Hou, J., Tsai, S., Li, R., Wang, J., Zhan, W., He, Z., Vajda, P., Keutzer, K., Tomizuka, M.: Nerf-det: Learning geometry-aware volumetric representation for multi-view 3d object detection. In: Proceedings of the IEEE/CVF International Conference on Computer Vision (ICCV). pp. 23320–23330 (October 2023) [2](#), [3](#), [4](#), [5](#), [6](#), [9](#), [10](#), [11](#), [12](#), [13](#)
41. Yariv, L., Gu, J., Kasten, Y., Lipman, Y.: Volume rendering of neural implicit surfaces. *Advances in Neural Information Processing Systems* **34**, 4805–4815 (2021) [4](#)
42. Yu, A., Ye, V., Tancik, M., Kanazawa, A.: pixelnerf: Neural radiance fields from one or few images. In: Proceedings of the IEEE/CVF Conference on Computer Vision and Pattern Recognition. pp. 4578–4587 (2021) [4](#)
43. Zhou, Y., Tuzel, O.: Voxelnet: End-to-end learning for point cloud based 3d object detection. In: Proceedings of the IEEE conference on computer vision and pattern recognition. pp. 4490–4499 (2018) [1](#)
44. Zhu, X., Su, W., Lu, L., Li, B., Wang, X., Dai, J.: Deformable detr: Deformable transformers for end-to-end object detection. *arXiv preprint arXiv:2010.04159* (2020) [2](#), [4](#)